Title	Pressure induced anisotropy of electrical conductivity in polycrystalline molybdenum disulfide
Authors	Sanchez, V.;Benavente, Eglantina;O'Dwyer, Colm;Lavayen, Vladimir;Santa-Ana, María A.;Sotomayor Torres, Clivia M.;Gonzalez, Guillermo
Publication date	2006-01
Original Citation	Sánchez, V., Benavente, E., Lavayen, V., O'Dwyer, C., Sotomayor Torres, C. M., González, G. and Santa Ana, M. A. (2006) 'Pressure induced anisotropy of electrical conductivity in polycrystalline molybdenum disulfide', Applied Surface Science, 252(22), pp. 7941-7947.
Type of publication	Article (peer-reviewed)
Link to publisher's version	http://www.sciencedirect.com/science/article/pii/S0169433205014753 - 10.1016/j.apsusc.2005.10.011
Rights	© 2006, Elsevier. NOTICE: this is the author's version of a work that was accepted for publication in Applied Surface Science. Changes resulting from the publishing process, such as peer review, editing, corrections, structural formatting, and other quality control mechanisms may not be reflected in this document. Changes may have been made to this work since it was submitted for publication. A definitive version was subsequently published in Applied Surface Science [252, 22, 15 September 2006] DOI: http://dx.doi.org/10.1016/j.apsusc.2005.10.011 - https://creativecommons.org/licenses/by-nc-nd/4.0/
Download date	2025-04-22 02:53:41
Item downloaded from	https://hdl.handle.net/10468/989

University College Cork, Ireland
Coláiste na hOllscoile Corcaigh

Pressure Induced Anisotropy of Electrical Conductivity in Polycrystalline Molybdenum Disulfide

V. Sánchez, [a] E. Benavente, [b] V. Lavayen, [c,*] C. O'Dwyer, [c]
C. M. Sotomayor Torres, [c] G. González [d]

[a] *Faculty of Science, Universidad Católica del Norte, Av. Angamos 0610, Antofagasta, Chile*

[b] *Department of Chemistry, Universidad Tecnológica Metropolitana, Av. Jose Pedro Alessandri, Santiago, Chile*

[c] *Tyndall National Institute, Lee Maltings, Prospect Row, Cork, Ireland*

[d] *Department of Chemistry, Faculty of Science, Universidad de Chile, P.O. Box 653, Santiago, Chile*

Abstract

Anisotropic specimens of MoS_2 are obtained by pressing the microcrystalline powder into special die. This inelastic compression results in a rearrangement of the disulfide micro platelets observed by Atomic Force Microscopy and reflected in the macroscopic anisotropy in electrical conductivity in these samples. The conductivity measured parallel and perpendicular to the direction of applied pressure exhibits an anisotropy factor of ∼10 at 1 GPa. This behaviour of the conductivity as a function of applied pressure is explained as the result of the simultaneous influence of a rearrangement of the micro platelets in the solid and the change of the inter-grain distances.

Key words: Anisotropy, Conductivity, Molybdenum, Surface pressure
PACS: 61.66.-f, 68.35.-p, 68.37.-d, 72.80.-r, 73.25.+i

* Corresponding author. Tel: + 353 21 490-4391; Fax: + 353 21 490-4467.
Email address: vlavayen@tyndall.ie (V. Lavayen,).

1 Introduction

A very relevant feature of molybdenum disulfide is its hexagonal layered structure, a characteristic that leads to its use as a lubricant [1], as a catalyst [2] and makes it an ideal material to explore intercalation chemistry [3]. Also the transport properties of MoS_2 are not an exception [4]. Pure MoS_2 is an intrinsic semiconductor with a marked anisotropic behaviour [3]. Single-crystal electrical conductivity along the axis perpendicular and parallel to the layer plane shows a ratio $\left(\frac{\sigma_{\parallel}}{\sigma_{\perp}}\right)$ of about 10^3 [5]. However, in spite of the relatively high anisotropy of layered transition metal disulfide, the use of these kinds of materials to develop, for instance, new electronic and electrochemical devices is often discouraged by the difficulties in obtaining single-crystals [6,7].

The fact that polycrystalline transition metal disulfides are rather more abundant and convenient than single crystal specimens, encourages us to study transport properties of these kinds of samples searching for conditions under which the anisotropy of the materials may be observed. Furthermore, such a procedure will be especially useful for intercalation host-guest derivatives of layered transition metal disulfides, which exhibit intrinsic anisotropic transport properties, typically superior to those of the pristine host, but they may be obtained only as microcrystalline powders [8].

In this paper, the microscopic ordering and the electrical conductivity behaviour of compressed polycrystalline samples of MoS_2 as a function of pressure and temperature is described, and a model describing the variations between the applied pressure and the anisotropy of the system is proposed. The dependence of the conductivity on the density of the material shows that after a given pressure, the sample can be considered as a pseudo single-crystal from its conductivity characteristics.

2 Experimental

Molybdenum disulfide (Aldrich 99%) was used as received without further treatment. Samples for electrical conductivity measurements were prepared by pressing the polycrystalline powder in a specially designed die to obtain parallelepiped pellets of about $5 \times 5 \times 2$ mm^3. The applied pressure was in the range of 50 MPa - 1 GPa. The density was determined from the weight and volume of the samples.

Atomic Force Microscopy (AFM) investigations were conducted on the faces of the die in directions parallel and perpendicular to that of the applied pressure. Examinations were conducted at room temperature in air using a Veeco

NanoScope IIIa MultiMode Scanning Probe Microscope. Scanning Tunnelling Microscopy (STM) characterization was conducted at a bias voltage of 80 mV and at 250 pA in constant current mode. The electrical measurements were performed with an Electrochemical Impedance Analyzer PAR model 6310 using ion blocking electrodes realised by sputtering a film of ∼30 nm of gold on opposite faces of the pellets.

3 Results and Discussion

3.1 Structural Characterisation of Compressed MoS_2

Manipulation of polycrystalline powders of layered compounds like MoS_2 often induces ordering of the micro crystals in the sample. Indeed, X-ray diffraction patterns obtained at the surface of such samples show reflection intensity ratios that differ from those obtained by transmission through the bulk [9].

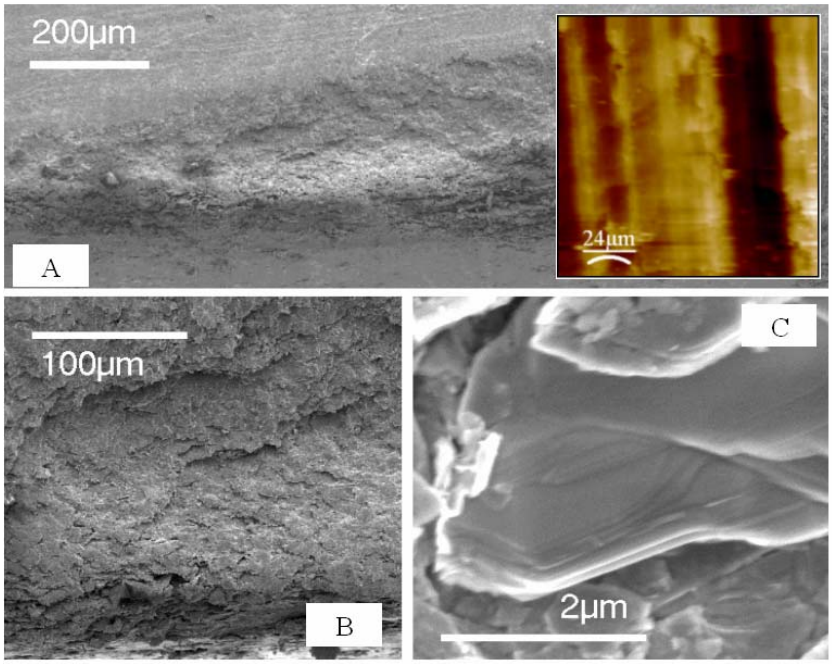

Fig. 1. SEM images of compressed molybdenum disulfide specimens of the surfaces (a) perpendicular and (b) parallel to the direction of applied pressure (c) Molybdenum disulfide powder. *inset* Tapping mode AFM image of the cross-section of two compressed platelettes of MoS_2. The lamellar structure is evident on the macro scale.

In the former case, the $\{00l\}$ plane reflections are notoriously enhanced due to spontaneous ordering taking place on the surface. This feature becomes

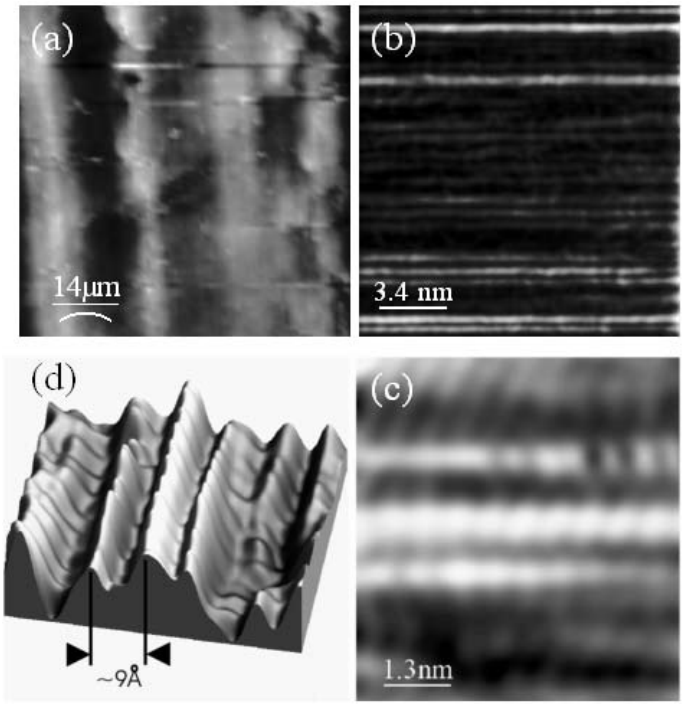

Fig. 2. (a-c) AFM images of a microcrystal of MoS_2 in a position perpendicular to the direction of applied pressure with various scan sizes. (d) Height profiles correspond to the expected periodicity in oriented micro-crystals. Both micro and nano-scale images show pronounced lamellar structuring.

more pronounced when the surface is flattened due to the increase in the number of micro lamellae oriented perpendicularly to the direction of the pressure. The same behaviour is expected for pellets prepared by pressing the microcrystalline powder, which can be clearly seen in the SEM images shown in Fig. 1.

The density of particles is greater in the lateral surface of the pellets than in the basal one. AFM also allows an analysis of the particles with a resolution in the nanometer scale. Results reproduced in Fig. 2 show that observed height profiles of adjacent lamellae correspond to the expected periodicity in oriented micro-crystals [3]. The sample preparation procedure used here provides, therefore, a valuable method for studying the structure of micro crystals at a quasi-atomic level.

In Fig. 3(a), we present atom-resolved STM data of the MoS_2 lamellar surface. It is immediately obvious that the surface has a high degree of crystallinity and has a three-fold packing arrangement comensurate with a hexagonal crystal structure. The protrusions in the image have a nearest-neighbour distance of $\sim$0.29 nm, evidenced by the line scan analysis presented if Fig. 3(b). This is exactly the distance of the reduced interatomic spacing of S atoms in the (0001) basal plane of MoS_2, which is a layered compound, consisting of stacks of S-Mo-S sandwiches held together by van der Waals interactions. Each sandwich

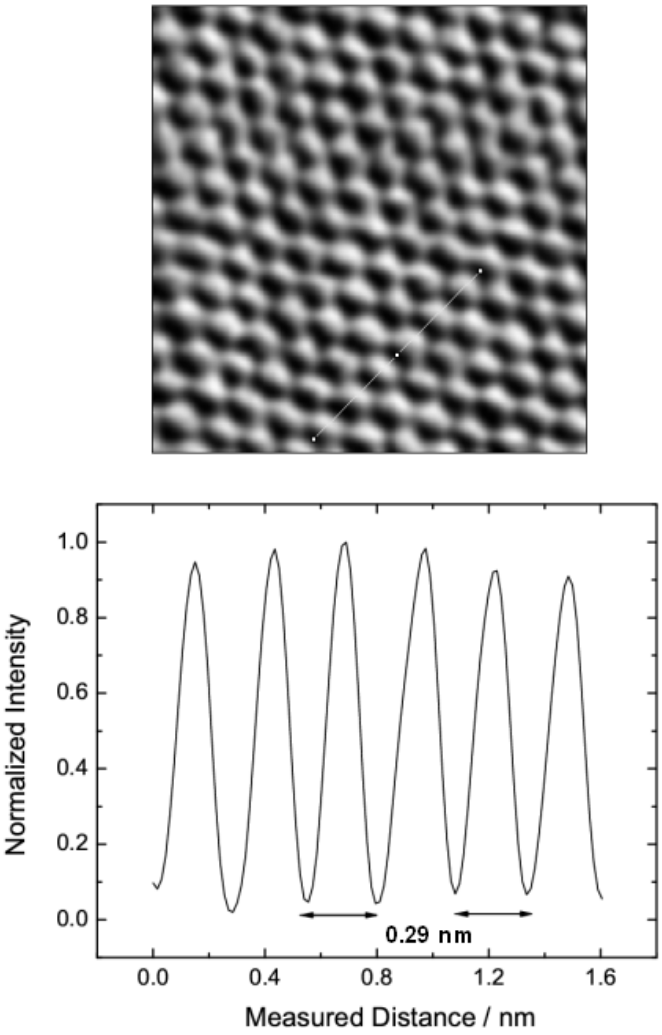

Fig. 3. (a) 3 nm × 3 nm constant current STM image of the MoS_2 surface showing the $(\sqrt{3a} \times \sqrt{3a})$ hexagonal packing arrangement of the outermost S atoms of the basal (0001) plane of the S-Mo-S stacked compound. (b) The corresponding cross-sectional line scan profile where the repeat distances, as a function of the reduced interatomic S-S distance, $a = 0.29$ nm, are also highlighted.

is composed of two hexagonal planes of S atoms and an intermediate hexagonal plane of Mo atoms, trigonal prismatically coordinated to the S atoms. It is important to point out that at low bias, constant current STM images reflect the local density of states at the Fermi level projected to the position of the tip apex [10,11]. In general, the images represent a convolution of the geometric and electronic structure of the surface. Since our STM images did not change by varying the tunnel current, we interpret the protrusions to reflect the hexagonally arranged S atoms in the topmost S layer of the (0001) surface of the MoS_2 lamellae. Thus, we can consider the compound as polycrystalline with a high degree of crystallinity for each crystal phase.

The density of microcrystalline MoS_2 powder was also measured and is ob-

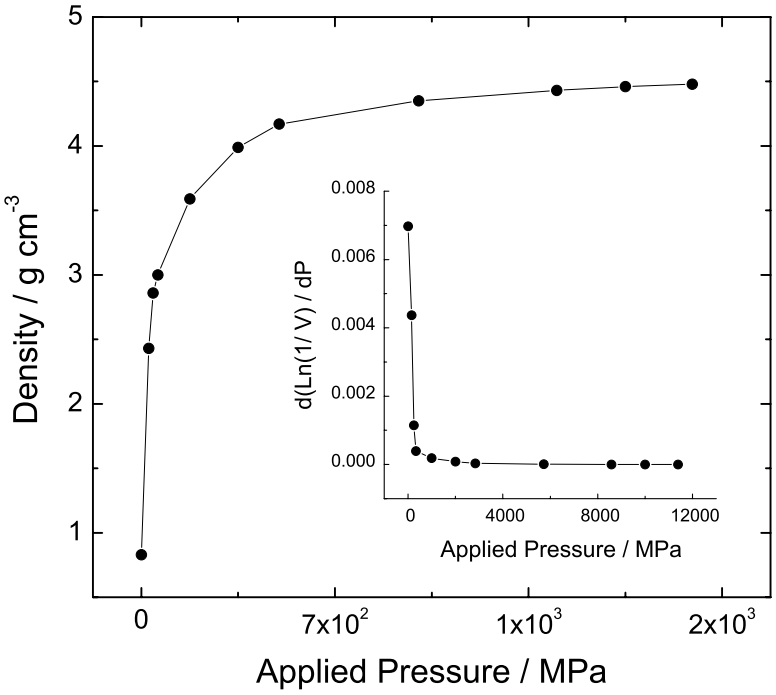

Fig. 4. Dependence of the density of a specimen of compressed MoS_2 on the applied pressure. *insert* The corresponding change of the 'pseudo-compressibility', $\frac{dL(1/V)}{dP}$ as a function of the applied pressure.

served to vary inelastically with pressure, as illustrated in Fig. 4. In the limit, it tends to that of the single crystal [12]. This behaviour is certainly related to a change in the packing of the micro lamellae and a corresponding increase in the degree of crystallinity in the sample.

An important contribution arises from the increase in order of the arrangement of the platelets in the sample, as indicated by the AFM measurements in Fig. 2. Another important factor is the decrease in the average distance between the particles. As shown by the change of $\frac{dL(1/V)}{dP}$ (see insert to Fig. 4), which can be considered as a pseudo-compressibility of the sample [8,13], it is apparent that at least two kinds of processes dominate the low and high pressure range.

The most interesting and important variation associated with the pressure in these MoS_2 samples is their electrical conductivity, which exhibits an anisotropic behaviour as shown in Fig. 5. In general, the conductivity is about one order of magnitude larger in the parallel direction to the layers, $\sigma_{\|}$ (horizontal σ), than in the perpendicular direction, $\sigma_{\perp}$ (vertical σ). The difference depends on both the pressure and the temperature. It is observed that $\sigma_{\|}$ increases with a corresponding increase in applied pressure, evident in Fig. 5. However, the variation of $\sigma_{\perp}$ appears to be relatively more complex in the range of ob-

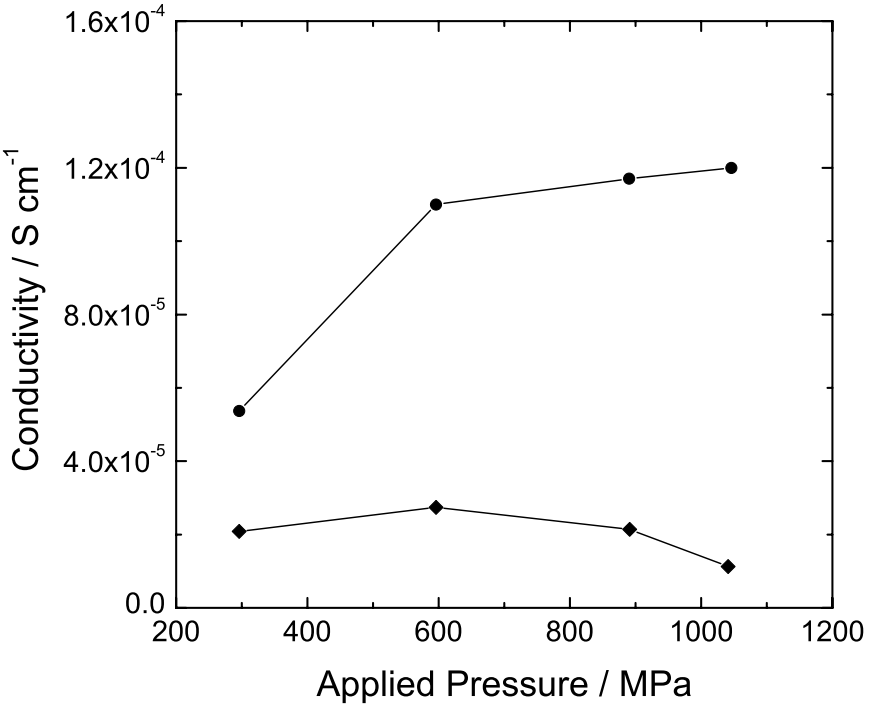

Fig. 5. Electrical conductivity measured parallel ($\sigma_{\parallel}$) -●- and perpendicular ($\sigma_{\perp}$) -◆- to applied pressure in compressed MoS_2.

servation (400-1000 MPa). Indeed the maximum conductivity reached is ∼10 times greater at this pressure (1 GPa).

As discussed above, two processes appear to be the most important regarding the changes in the physical properties of compressed pellets. One of these, the anisotropic electrical conductivity, is controlled by the orientation of the grains and the average distance between them. Starting with a statistical orientation of the grains when pressure is applied, the resistance of the system can be represented as an equivalent circuit formed with two resistors $R_{\parallel}$ (the parallel resistance) and $R_{\perp}$ (perpendicular resistance). These impedances define the system in the direction of the applied pressure (parallel and perpendicular directions respectively). These two circuit elements form part of the anisotropic resistance and are proportional to the applied pressure and direction of the pressure in the system. Furthermore, the anisotropic resistances are proportional to the inter-particle resistance (R_{ip}), and the total resistance is the sum of each component in the system [14], illustrated by the equivalent circuit in Fig. 6.

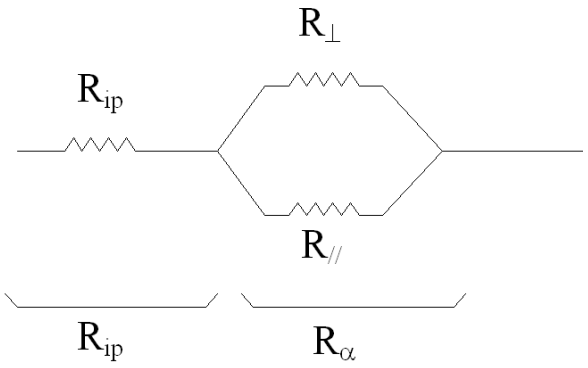

Fig. 6. Equivalent circuit representation of the inter-particle resistance (R_{ip}) and anisotropic resistance (R_a) together with the perpendicular ($R_\perp$) and parallel ($R_\parallel$) anisotropic resistances.

3.2 Modelling the Anisotropic Conductivity

We now present a model to discuss the results and propose an analysis of the measured conductivity in samples compressed in parallel and perpendicular directions. We have classified the system with three important factors arising from the behaviour of the conductivity as a function of the applied the pressure in the system:

- The inter-particle distance
- Degree of preferred orientation of the layers
- Values of the parallel and perpendicular conductivity in the samples

In samples where low pressure was applied, we assume that the inter-particle distances are high and that the conductivity will be a function of the probability of electron promotion within the particles [13]. Secondly, when the inter-particle resistance decreases, the degree of preferred orientation becomes an important factor. If the sample presents a value that tends to zero in the inter-particle resistance, R_{ip} (parallel system), with its micro-lamellae statistically positioned, then the total resistance (R_T) can be expressed by *eq* 1 [13] and the total conductivity (σ_T) is given by the relationship between the resistivity and electrical conductivity in *eq* 2.

$$R_T = R_{ip} + R_\alpha \tag{1}$$

$$\sigma_T = \frac{\sigma_{ip}\sigma_\alpha}{(\sigma_{ip} + \sigma_\alpha)} \tag{2}$$

where σ_{ip} is the inter-particle conductivity and σ_{α} is the anisotropic conductivity.

The anisotropic conductivity (σ_{α}) can be defined as a vector [14] dependent on the orientation θ between the laminae of MoS_2, where θ is a function of the applied pressure. The magnitude of this vector ($\sigma_{\circ}$) is the total value of the anisotropic conductivity. This vector has two components that are a function of the angle of orientation (θ), namely, the horizontal intrinsic conductivity ($\sigma_{\alpha ih}$) and the vertical intrinsic conductivity ($\sigma_{\alpha iv}$), given by *eq* 3,

$$\sigma_{\alpha} = \sigma_{\alpha ih} + \sigma_{\alpha iv} \tag{3}$$

To further understand these relations, we note that the pressure is zero when the anisotropic angle has a value of $\left(\frac{\pi}{4}\right)$ rad and at an angle of 0 rad, the pressure tends to infinity. Thus it is possible to define the horizontal intrinsic conductivity ($\sigma_{\alpha ih}$) and the vertical intrinsic conductivity ($\sigma_{\alpha iv}$) as a function of the angle (θ) by *eqs* 4 and 5 and the dependencies are plotted in Fig. 7.

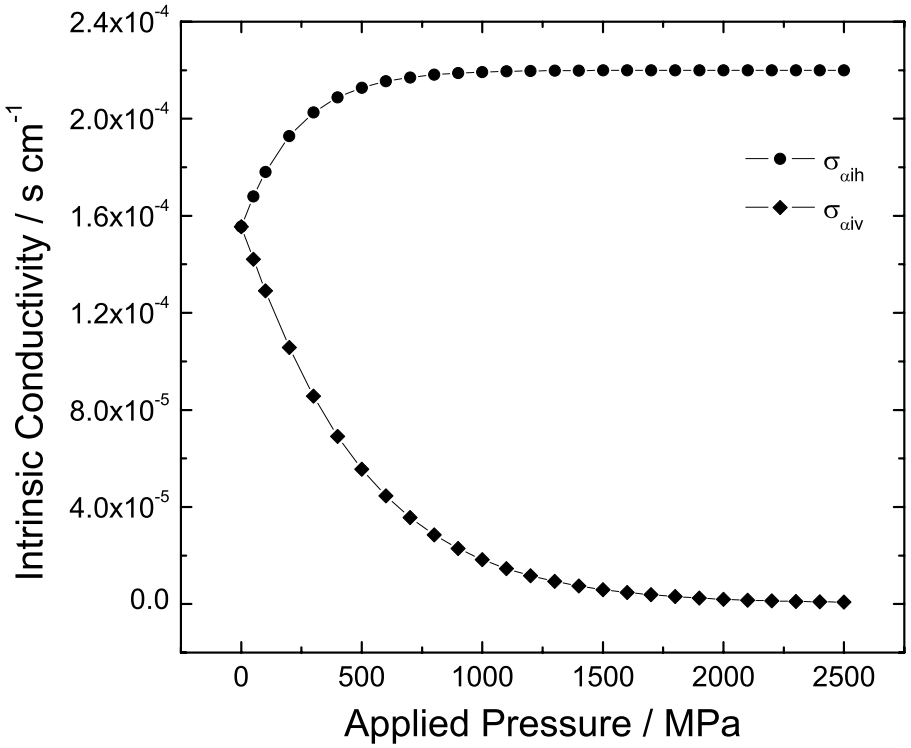

Fig. 7. Simulated curves of the intrinsic horizontal conductivity ($\sigma_{\alpha ih}$) and intrinsic vertical conductivity ($\sigma_{\alpha iv}$) as a function of applied pressure.

$$\sigma_{\alpha ih} = \{(\sigma_{\circ\parallel} \cos\theta)^2 + (\sigma_{\circ\perp} \sin\theta)^2\}^{1/2} \tag{4}$$

$$\sigma_{\alpha iv} = \{(\sigma_{\circ\parallel} \sin\theta)^2 + (\sigma_{\circ\perp} \cos\theta)^2\}^{1/2} \tag{5}$$

with $0 \leqslant \theta \leqslant \left(\frac{\pi}{4}\right)$. The determination of the inter-particle conductivity (σ_{ip}) is possible when the pressure tends to zero. Analysing the conductivity of the system at low pressure, we find that the behaviour of the system is similar in both perpendicular and parallel directions and follows a linear behaviour. This behaviour implies a proportional relation between the conductivity and the pressure, given by *eqs* 6 and 7.

$$\sigma_{ip\parallel} = c_\parallel + K_\parallel \cdot P \tag{6}$$

$$\sigma_{ip\perp} = c_\perp + K_\perp \cdot P \tag{7}$$

where $K_\parallel$ and $K_\perp$ are the gradients of *eqs* 4 and 5 respectively, and P is the applied pressure vector.

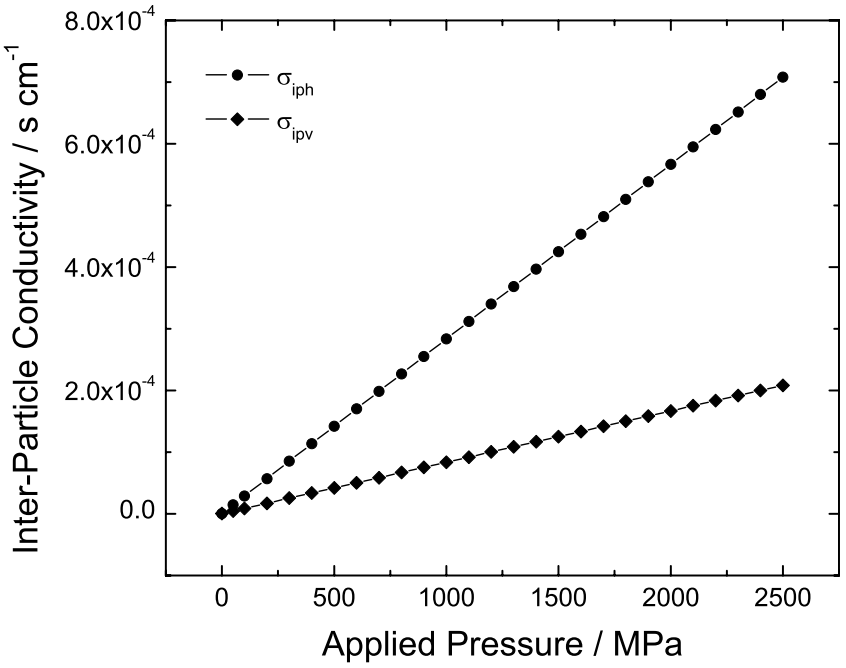

Fig. 8. Simulated curves of perpendicular and parallel inter-particle conductivity as a function of the applied pressure in the system. Both curves can be represented by the following relations: $\sigma_{iph} = 3\times10^{-7}(P) - 4\times10^{-7}$ and $\sigma_{ipv} = 8\times10^{-8}(P) - 4\times10^{-7}$

On increasing the pressure in the system we find that this linear behaviour changes because the inter-particle distance reduces, as evident from Fig. 8.

This inter-particle distance reduction implies that the parallel and perpendicular inter-particle conductivities diverge when the pressure tends to infinity (effectively at high pressures of ∼1 GPa). A linear behaviour is observed when the pressure tends to zero (at low pressures of ∼50 MPa or less).

When correlated, the experimental and theoretical values for the conductivity can be expressed by *eqs* 8 and 9, resulting from dilution of *eq* 2 by *eqs* 4 and 6 for the parallel case and for the perpendicular case we find good agreement between the theoretical and experimental values, shown in Fig. 9.

$$\sigma_{T\parallel} = \frac{\left(c_\parallel + K_\parallel \cdot P\right)\left\{\left(\sigma_{\circ\parallel}\cos\theta\right)^2 + (\sigma_{\circ\perp}\sin\theta)^2\right\}^{1/2}}{\left(c_\parallel + K_\parallel \cdot P\right) + \left\{\left(\sigma_{\circ\parallel}\cos\theta\right)^2 + (\sigma_{\circ\perp}\sin\theta)^2\right\}^{1/2}} \tag{8}$$

$$\sigma_{T\perp} = \frac{(c_\perp + K_\perp \cdot P)\left\{\left(\sigma_{\circ\parallel}\sin\theta\right)^2 + (\sigma_{\circ\perp}\cos\theta)^2\right\}^{1/2}}{(c_\perp + K_\perp \cdot P) + \left\{\left(\sigma_{\circ\parallel}\sin\theta\right)^2 + (\sigma_{\circ\perp}\cos\theta)^2\right\}^{1/2}} \tag{9}$$

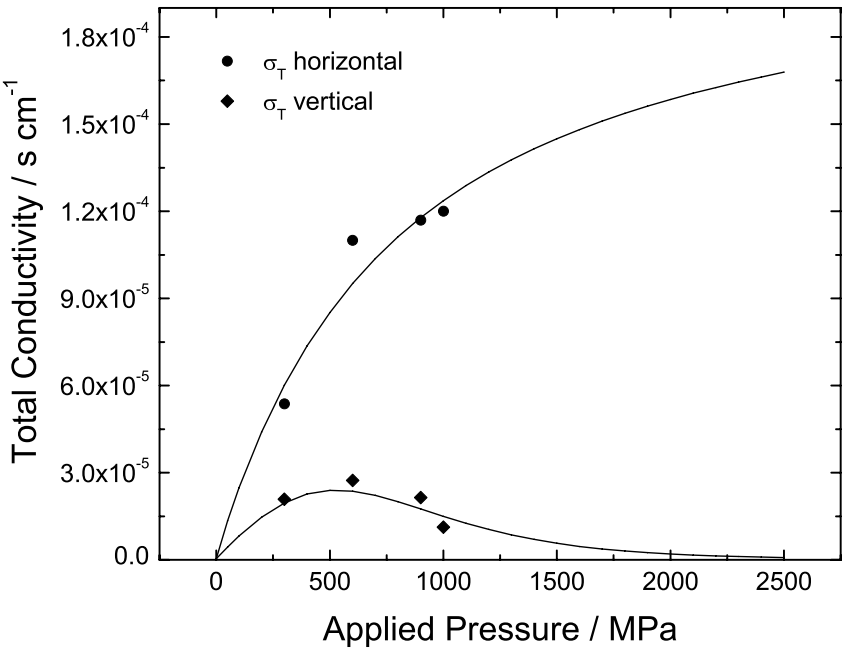

Fig. 9. Correlation of the simulated curves to the total electrical conductivity ($\sigma_{T\parallel}$ and $\sigma_{T\perp}$), calculated using theoretical and experimentally determined data for molybdenum disulfide. The solid lines are the theoretical profiles with experimental data points overlaid for comparison.

The conductivity as a function of the temperature was also studied and the results are presented in Fig. 10. The data indicate that the MoS_2 samples exhibit semiconductor behaviour in both cases, *i.e.*, the conductivity increases with temperature. Arrhenius plots show a near-linear behaviour in almost all cases, from which the activation energy for the processes may be estimated. In the case of $\sigma_\perp$, the slopes of the Arrhenius plots have practically the same value, estimated to be ∼0.6 eV, which in turn is approximately the same as that observed for $\sigma_\parallel$.

We observe that the dependence on temperature follows an Arrhenius behaviour and in almost all cases we find that the relation follows a near-linear tendency (as shown in Fig. 10), with a value of the activation energy estimated to be ∼0.6 eV. This observation implies that the conduction mechanism as a function of temperature is similar in both directions.

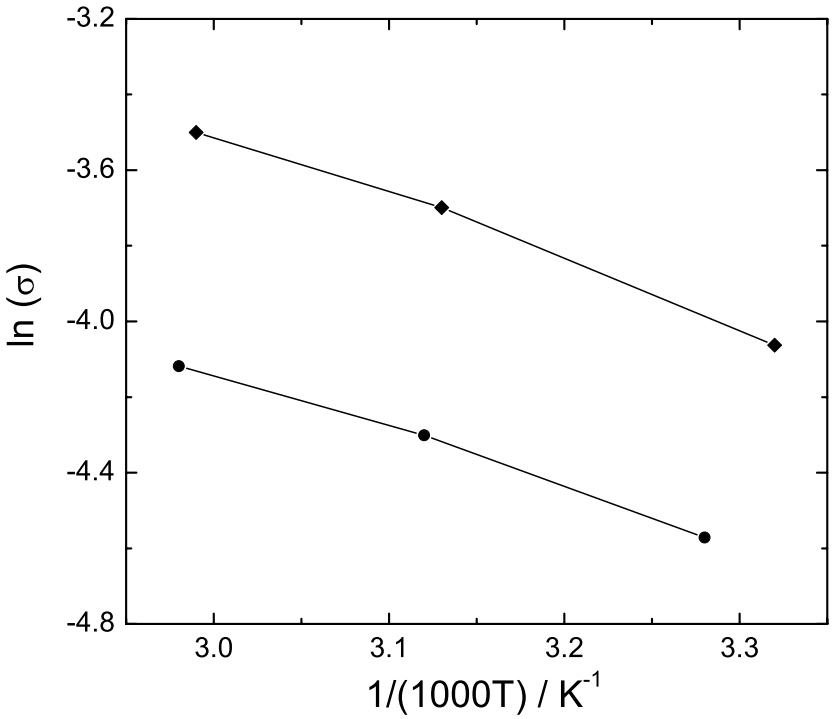

Fig. 10. Experimentally measured electrical conductivity of the parallel ($\sigma_\parallel$) -♦- and perpendicular ($\sigma_\perp$) -•- directions as a function of the temperature of molybdenum disulfide in a specimen prepared at 1 GPa.

Employing the model described in section 3.2 and assuming that in a system

with high order (low pressure), and an inter-particle resistance (R_{ip}) that is much less than the anisotropic resistance (R_a), then we do not have to consider the inter-grain factor. Then using *eqs* 4 and 10, we can obtain values for the horizontal intrinsic conductivity ($\sigma_{\alpha ih}$) and also for the vertical intrinsic conductivity ($\sigma_{\alpha iv}$) using *eqs* 5 and 11, taking into consideration that the parallel and perpendicular activation energies are equivalent.

$$\sigma_{\alpha ih} = C_{\parallel} \exp\left(\frac{-E_{a\parallel}}{RT}\right) \tag{10}$$

$$\sigma_{\alpha iv} = C_{\perp} \exp\left(\frac{-E_{a\perp}}{RT}\right) \tag{11}$$

On comparison of the theoretical model and the experimental results, the model that we propose exhibits divergence due primarily to the ratio of the activation energies $\left(\frac{E_{a\perp}}{E_{a\parallel}}\right)$ being non-unity.

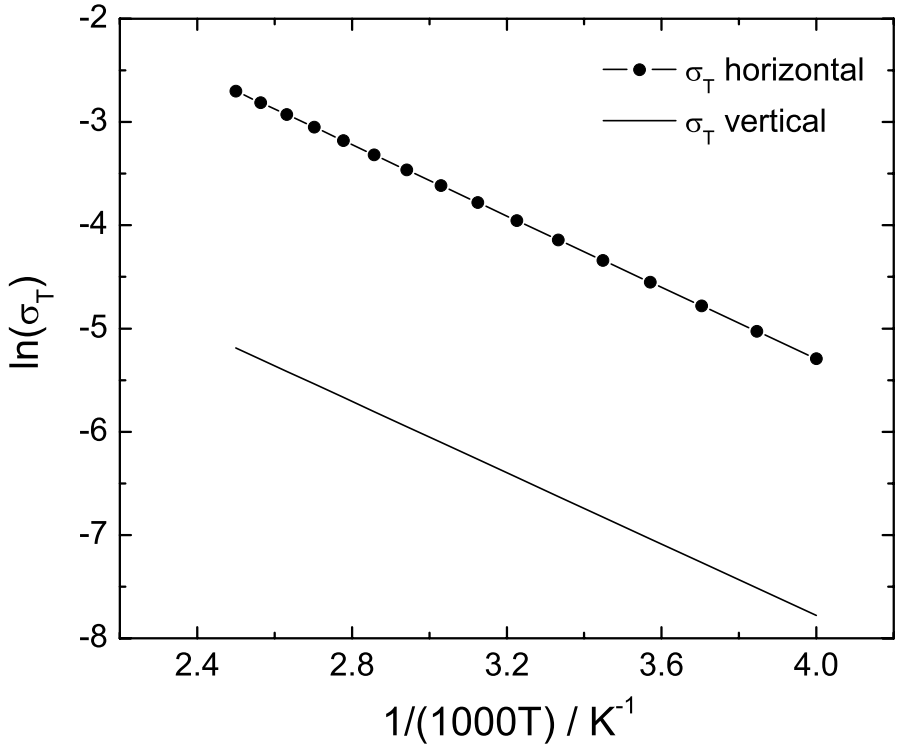

Fig. 11. Correlation of the simulated curves to the total conductivity, calculated using theoretical and experimental values as a function of the temperature for molybdenum disulfide with $\left(\frac{E_{a\perp}}{E_{a\parallel}}\right) = 2.9$.

For example, the variation of the total conductivity with temperature at low

pressure shows marked divergence when the ratio of activation energies is non-unity, shown in Fig. 11. No divergence is observed for one special case: when the activation energy ratio is unity. We find that, in general, the ratio of activation energies, $\left(\frac{E_{a\perp}}{E_{a\parallel}}\right)$, varies with temperature according to Fig. 12. Considerable divergence is noted at temperatures greater than $\sim$340° C for a given pressure of $\sim$1 GPa. Taking the values of horizontal intrinsic conductivity ($\sigma_{\alpha ih}$) and vertical intrinsic conductivity ($\sigma_{\alpha iv}$) we find different ratios of $\left(\frac{E_{a\perp}}{E_{a\parallel}}\right)$ and we observe a markedly different behaviour to that observed in the experimental observations, at ratio divergences of $\sim$10%.

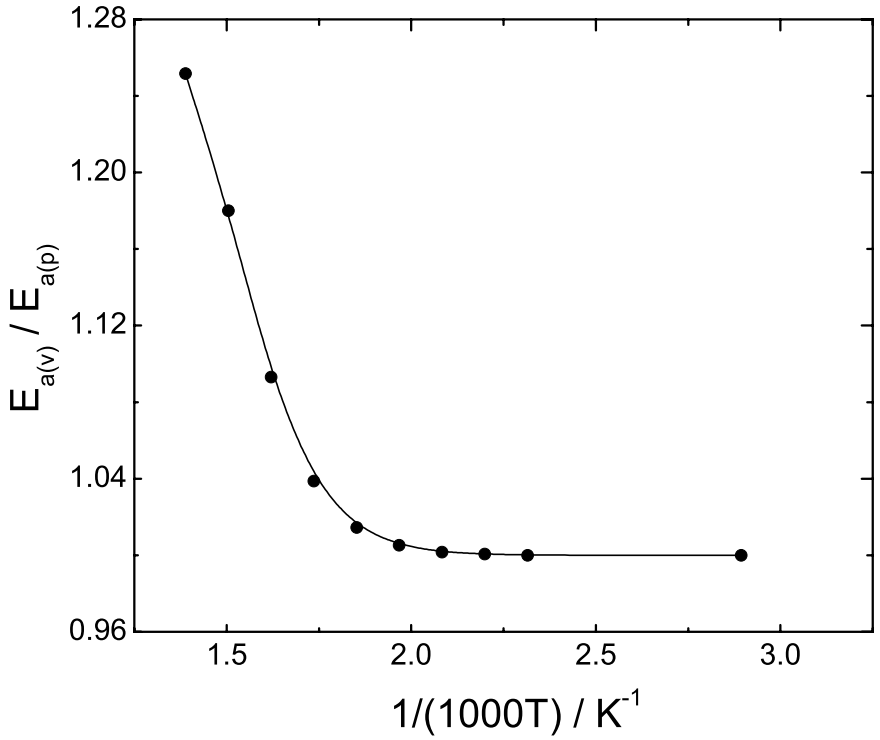

Fig. 12. Simulated curve of the activation energy ratio $\left(\frac{E_{a\perp}}{E_{a\parallel}}\right)$ as a function temperature for molybdenum disulfide.

Considering the system at high pressure, the inter-particle resistance increases dramatically and the anaytical system becomes much more complex. This situation is currenty under study and results will be presented in a future publication.

4 Conclusions

Results discussed above show that for microcrystalline samples of MoS_2 lamellar solids become ordered by pressure leading to specimens in which the intrinsic anisotropy of the micro crystals is to some degree macroscopically observed. In the case of polycrystalline MoS_2 an anisotropy factor of $\sim$10 is obtained at 1 GPa and the electrical conductivity in the direction parallel to the lamellae is also measured to be $\sim$10 times that in the perpendicular direction.

It may be assumed that the electrical conductivity observed in both directions, at least at relatively low and medium pressures, corresponds almost entirely to the contribution to the platelets oriented parallel to the direction of applied pressure. However, the resistance associated with the inter-grain distance will be different for particles oriented parallel or perpendicularly to each other. The contribution of inter-grain resistance observed in the conductivity of pressed pellets can be considered, as a first approximation, identical in both directions. Also, the similarity of activation energies in both directions, estimated from the dependence of the conductivity on the temperature, agrees with such an interpretation.

The different behaviour of $\sigma_{\parallel}$ and $\sigma_{\perp}$ as a function of pressure can be also explained by considering the approach discussed above. In the case of parallel conductivity, both re-orientation of the lamellae and the reduction of the inter-grain distance induced by the applied pressure tend to enhance the conductivity, so a continuous increase of $\sigma_{\parallel}$ is observed.

In the perpendicular direction, by comparison, the decrease of the inter-grain distance tends to increase the conductivity but the reorganization of the lamellae produces the contrary effect. The former factor appears to be the most important at low pressure inducing an initial increase of the conductivity.

Acknowledgements

The support of the Science Foundation Ireland, the University of Chile and Fondecyt (Grant 1050344) is gratefully acknowledged.

References

[1] S. Watanabe, J. Noshiro and S. Miyake, Surf. Coat. Techn. 183, (2004) 347. (b) X. Zhu, W. Lauwerens, P. Cosemans, M. Van Stappen, J. P. Celis, L. M. Stals. Jiawen He, Surf. Coat. Techn. 163-164 (2003) 422.

[2] C. Xiangying, W. Xiong, W. Zhenghua, Y. Weichao, Q. Yitai, Mater. Chem. Phys. 87 (2004) 327. (b) S. Mingyong, J. Adjaye. A. E. Nelson, App. Catal. A. Gen. 263 (2004) 131.

[3] N. Mirabal, P. Aguirre, M. A. Santa Ana, E. Benavente, G. González, Electrochimica Acta, 48 (2003) 2123. (b) E. Benavente, M. A. Santa Ana, F. Mendizábal, G. González, Coord. Chem. Rev. 224 (2002) 87. (c) F. Mendizábal, M. A. Santa Ana, E. Benavente, G. González, J. Chil. Chem. Soc, 48 (2003) 69. (d) A. C. Bloise, J. P. Donoso, C. J. Magon, J. Schneider, H. Panepucci, E. Benavente, V. Sánchez, M. A. Santa Ana, G. González, J. Phys. Chem. B, 106, (2002) 11698.

[4] E. Beqqali, I. Zorkani, F. Rogemond, H. Chermette, R. B. Chaabane, M. Gamoud. G. Guillaud, Synthetic Metals, 90 (1997) 165. (b) M. A. Santa-Ana, V. Sanchez. G. Gonzalez, Electrochimica Acta, 40 (1995), 1773. (c) V. R. K. Sastry, S. D. Phatak and A. Sethuramiah, Wear, 86 (1983) 213.

[5] A. M. Hermann, R. Samoano, V. Hadek, A. Rembaum, Solid. State. Comm, 13 (1973) 1065. (b) J. A. Woollam, R. B. Samoano, Mat. Sci. Eng., 31 (1977) 289. (c) J. K. Lancaster, Wear, 9 (1966) 169. (d) V. Sánchez, E. Benavente, M. A. Santa Ana, G. González, Chem. Mater. 11, (1999) 2296.

[6] K. T. Park, M. Richards-Babb, M. S. Freund, J. Weiss, K. Klier, J. Phys. Chem. 100 (1996) 10739.

[7] J. Heising, M. G. Kanatzidis, J. Am. Chem. Soc. 121 (1999) 638.

[8] J. A. Kornblatt, E. B. Sirota, H. E. King, Jr., R. H. Baughman, C. Cui, S. Stafstrom, S. O. Dantas, Science, 143 (1998) 281. (b) R. H. Baughman, S. Stafstrom, C. Cui, S. O. Dantas, Science, 279 (1998) 1522.

[9] Hui-Lien Tsai, J. Heising, J. L. Schindler, C. R. Kannewurf., M. G. Kanatzidis, Chem. Mater, 9 (1997) 879.

[10] J. Tersoff and D. R. Hamann, Phys. Rev. B, 31 (1985) 805.

[11] C. O'Dwyer, G. Gay, B. Viaris de Lesegno and J. Weiner, Langmuir, 20 (2004) 8172.

[12] H. Tang. R. Morrison, Thin Solid Films, 227 (1993) 94. (b) R. Divigalpitiya, S. R. Morrison, R. F. Frindt, Thin Solid Films, 186 (1990) 177.

[13] J. M. Albella, A. M. Cintas, T. Miranda, J. M. Serratosa editors, Introducción a la Ciencia de Materiales, Editorial C.S.I.C., 1993. (b) J. R. Macdonald, Impedance Spectroscopy, John Wiley & Sons, 1987.

[14] R. T. Johnson Jr, R. K. Quinn, J. Non Crys. Sol, 28 (1978) 273. (b) H. Tang, S. R. Morrison, Thin Solid Films, 227 (1993) 90.